Deterministic and statistical characterization of rigid frame porous materials from impedance tube measurements

M. Niskanen,[a] J.-P. Groby, A. Duclos, and O. Dazel
Laboratoire d'Acoustique de l'Universite du Maine (LAUM), UMR-6613 CNRS, Avenue Olivier Messiaen, Le Mans Cedex 9, F-72085, France

J. C. Le Roux and N. Poulain
Centre de Transfert de Technologie du Mans, 20 rue Thalès de Milet, Le Mans, F-72000, France

T. Huttunen and T. Lähivaara
Department of Applied Physics, University of Eastern Finland, P.O. Box 1627, Kuopio, FIN-70211, Finland

(Received 22 June 2017; revised 4 October 2017; accepted 6 October 2017; published online 27 October 2017)

A method to characterize macroscopically homogeneous rigid frame porous media from impedance tube measurements by deterministic and statistical inversion is presented. Equivalent density and bulk modulus of the samples are reconstructed with the scattering matrix formalism, and are then linked to its physical parameters via the Johnson–Champoux–Allard–Lafarge model. The model includes six parameters, namely the porosity, tortuosity, viscous and characteristic lengths, and static flow and thermal permeabilities. The parameters are estimated from the measurements in two ways. The first one is a deterministic procedure that finds the model parameters by minimizing a cost function in the least squares sense. The second approach is based on statistical inversion. It can be used to assess the validity of the least squares estimate, but also presents several advantages since it provides valuable information on the uncertainty and correlation between the parameters. Five porous samples with a range of pore properties are tested, and the pore parameter estimates given by the proposed inversion processes are compared to those given by other characterization methods. Joint parameter distributions are shown to demonstrate the correlations. Results show that the proposed methods find reliable parameter and uncertainty estimates to the six pore parameters quickly with minimal user input. © *2017 Acoustical Society of America*.
https://doi.org/10.1121/1.5008742

[MV] Pages: 2407–2418

I. INTRODUCTION

Models for sound propagation in porous media require the knowledge of several pore parameters.[1] Due to the numerous applications of these models (not limited to just acoustics), the problem of porous media characterization has received considerable interest.[2] Although there are ways to measure many of the pore parameters directly,[3–6] the methods require specialized equipment and are often difficult to carry out. Indirect acoustic methods, where the pore parameters are inferred from the measurement of the material's acoustic behavior, are an attractive alternative to direct measurements. This is because they offer a way to characterize the porous media using commonly found apparatus, such as an impedance tube or an ultrasonic measurement system. Indirect methods can be categorized into inverse methods[7–9] and into approaches that use analytical expressions[10–13] to solve the parameters.

Inverse characterization methods are especially interesting since they enable simultaneous estimation of several parameters. The methods consist of fitting a model describing the porous medium to a measurement, thus finding the parameters that best describe the medium. The semi-phenomenological model of Johnson–Champoux–Allard–Lafarge[14–16] (JCAL) is nowadays widely used for this purpose since it has proved robust and accurate in describing sound propagation in porous media over a large frequency range. The JCAL model relates the density and bulk modulus of the equivalent fluid in a rigid frame porous material to six pore parameters, namely porosity, tortuosity, viscous and thermal characteristic length, and viscous and thermal permeability. This kind of method was used by Atalla and Panneton,[7] where tortuosity and viscous and thermal characteristic lengths were recovered from surface impedance measurements after measuring the porosity and flow resistivity directly. Later Zieliński[9] recovered all six JCAL parameters from surface impedance measurements, with the help of normalized dimensionless parameters. In both works, an optimization algorithm was used to minimize a cost function, giving a set of pore parameters as a solution.

Although the area of porous material characterization is heavily researched, questions such as reproducibility of the measurements and reliability of the parameter estimates still remain. Inter-laboratory tests have shown that the reproducibility of acoustic properties between laboratories can be poor.[17,18] Uncertainties in the measurements translate to uncertainties in the pore parameter estimates, especially if the problem is ill-posed, and if they cannot be quantified, the solution might not be of much use. Moreover, all parameters

[a]Electronic mail: matti.niskanen@univ-lemans.fr

might not even be identifiable due to an insufficient frequency range and be highly correlated with each other. In addition, being trapped in a local minimum is an issue of all iterative solvers.

To understand better the ill-posedness and uncertainties in the inverse problem, the inversion can be performed in the Bayesian (statistical) framework,[19] which presents several advantages over deterministic parametric inversion methods. These include the ability to take into account knowledge of the measurement uncertainties, and prior information (such as literature values or characterization results from other methods). The solution of a statistical inverse problem is a probability density of all the parameters of interest. From this density, one can see if the problem has several minima, so that the most likely pore parameter values, the width of their density and relationships between the parameters, can be accurately estimated. This helps to reveal problems with identifiability related to parameter correlation. An example of statistical pore parameter inversion can be found in Chazot *et al.*,[8] where the five parameters of the JCA model (JCAL model without the thermal permeability introduced by Lafarge), and three elastic parameters were estimated from impedance tube measurements.

In this paper, we perform the inversion essentially in the same framework and using Markov chain Monte Carlo (MCMC) sampling as Chazot *et al.*,[8] but with a few important differences. First, we invert the parameters from two different points of view, deterministic (non-linear least squares) and statistical, because it is useful to quantify whether the solutions returned by a deterministic optimization algorithm are still usable after examining them with the added knowledge of parameter uncertainties and correlations. For Bayesian inversion, we estimate the measurement variance from repeated measurements, which also account for the possible inhomogeneities in the samples. In addition, we adopt an adaptive sampling scheme[20,21] for the MCMC, which frees the user from having to tune the chain parameters by hand. Importantly, we systematically check and present every one-dimensional and combinations of the two-dimensional marginal posterior densities, which reveal any correlations between parameters. To measure the material's equivalent density $\tilde{\rho}_{\mathrm{eq}}$ and bulk modulus $\tilde{K}_{\mathrm{eq}}$, we use a transmission impedance tube set-up,[22] with a semi-anechoic ending. We adopt the scattering matrix[23] formalism which allows for avoiding the effect of the necessarily existing backward propagating wave reflected from any anechoic termination, and simplifies the calculation of $\tilde{\rho}_{\mathrm{eq}}$ and $\tilde{K}_{\mathrm{eq}}$. The cost function is then formed by comparing the measured and modeled $\tilde{\rho}_{\mathrm{eq}}$ and $\tilde{K}_{\mathrm{eq}}$ directly, which separates the viscous and thermal pore parameters, leading to reduced correlation between them. We also discuss the potential advantages and disadvantages of inversion based on a simpler measurement of just the reflection coefficient with a rigid backing.

The paper is outlined in the following way: The JCAL model is recalled in Sec. II. Section III outlines the measurement set-up and the scattering matrix formulation. The deterministic and statistical inversion methods are introduced in Sec. IV. In Sec. V, the methods are applied to real measurements and compared to other characterization methods. The inverse problem is discussed in Sec. VI followed by a brief conclusion.

II. MODELING OF THE POROUS MEDIA

Acoustic energy in porous media is dissipated mainly through viscous and thermal losses, resulting from the interaction between the frame and the fluid. When the saturating fluid (in this case air) and the material frame are decoupled, the frame remains rigid and the porous medium can be represented as an equivalent fluid whose density and bulk modulus are defined by the pore structure.[1] The JCAL model describes this relation between pore parameters and the equivalent fluid bulk properties. In the model, the viscous losses are accounted for in the equivalent dynamic density, and thermal losses in the equivalent dynamic bulk modulus.

The equivalent density of the porous medium can be written as

$$\tilde{\rho}_{\mathrm{eq}} = \frac{\rho_0}{\phi}\tilde{\alpha}(\omega), \tag{1}$$

where ρ_0 is the density of the saturating fluid, ϕ the open porosity, and $\tilde{\alpha}(\omega)$ the dynamic tortuosity. The tilde over the functions indicates that they are complex and frequency-dependent. The equivalent bulk modulus can be written in a similar fashion as

$$\tilde{K}_{\mathrm{eq}} = \frac{\gamma P_0}{\phi}\left(\gamma - \frac{\gamma - 1}{\tilde{\alpha}'(\omega)}\right)^{-1}, \tag{2}$$

where P_0 is the static pressure and γ the specific heat ratio. The parameter $\tilde{\alpha}'(\omega)$ has been defined as a homologue to $\tilde{\alpha}(\omega)$, representing the thermal tortuosity.[16]

In the models that follow, the terms representing the fluid flow and thermal resistance of the material can be written using the flow and thermal resistivities σ and σ', or with the viscous static and thermal permeabilities k_0 and k_0', respectively. As shown in Appendix A, the formulations are mathematically identical, but the use of the permeability representation is physically more elegant as it does not mix the viscous and thermal parameters.

The Johnson *et al.*[14] model describes the dynamic density of a porous medium, where adopting the $e^{-\mathrm{i}\omega t}$ convention, the dynamic tortuosity is written as

$$\tilde{\alpha}(\omega) = \alpha_\infty + \frac{\mathrm{i}\nu}{\omega}\frac{\phi}{k_0}\sqrt{1 - \frac{\mathrm{i}\omega}{\nu}\left(\frac{2\alpha_\infty k_0}{\phi\Lambda}\right)^2}. \tag{3}$$

Here $\nu = \eta/\rho_0$ is the kinematic viscosity of the saturating fluid, η is the dynamic viscosity, and α_∞, Λ, and k_0 are the geometrical tortuosity, viscous characteristic length, and viscous static permeability of the porous medium, respectively.

The Champoux–Allard–Lafarge[15,16] model describes the dynamic bulk modulus of a porous medium. In this model, the thermal tortuosity is written as

$$\tilde{\alpha}'(\omega) = 1 + \frac{\mathrm{i}\nu'}{\omega}\frac{\phi}{k_0'}\sqrt{1 - \frac{\mathrm{i}\omega}{\nu'}\left(\frac{2k_0'}{\phi\Lambda'}\right)^2}, \tag{4}$$

where $\nu' = \nu/\mathrm{Pr}$, where Pr is the Prandtl number, Λ' is the thermal characteristic length, and k_0' is the static thermal permeability.

III. MEASUREMENT CONFIGURATION

The scattering matrix, which contains the reflection and transmission coefficients R and T of a homogeneous symmetric plate, can be recovered from four-microphone impedance tube measurements. Then $\tilde{\rho}_{\mathrm{eq}}$ and $\tilde{K}_{\mathrm{eq}}$ can be calculated straightforwardly.[13,24]

Figure 1 depicts the impedance tube and the two measurement set-ups used in this work. In set-up A, there are two 1/4 in. G.R.A.S. microphones on both sides of the sample and the tube ends with an anechoic end. In set-up B, the ending is changed to a tube where a movable piston acting as a rigid backing can be placed behind the sample. Diameter of the tube was 30 mm and the distance between the microphones 1–2 and 3–4 was 20 mm. Distance from microphone 2 to the sample surface was 30 mm, and the distance from the sample surface to microphone 3 was 150 mm. The excitation signal was a logarithmic swept sine, over the frequency range of 300–5800 Hz.

In both set-ups, the measurements can be performed with either a single or multiple microphones.[22] When using several microphones, they must be first calibrated and phase matched with each other to achieve accurate results, whereas when using a single microphone, there is naturally no need for calibration. The downside of using just a single microphone is that it needs to be moved to different locations to make a measurement.

A. Set-up A

The measured sound pressures P_j at locations x_j, $j = 1, 2, 3, 4$, can be related to the amplitudes of the standing waves p inside the tube with following equations:

$$P_1 = p_i^+ e^{\mathrm{i}k_t x_1} + p_0^+ e^{-\mathrm{i}k_t x_1}, \tag{5a}$$

$$P_2 = p_i^+ e^{\mathrm{i}k_t x_2} + p_0^+ e^{-\mathrm{i}k_t x_2}, \tag{5b}$$

$$P_3 = p_o^- e^{\mathrm{i}k_t x_3} + p_i^- e^{-\mathrm{i}k_t x_3}, \tag{5c}$$

$$P_4 = p_o^- e^{\mathrm{i}k_t x_4} + p_i^- e^{-\mathrm{i}k_t x_4}. \tag{5d}$$

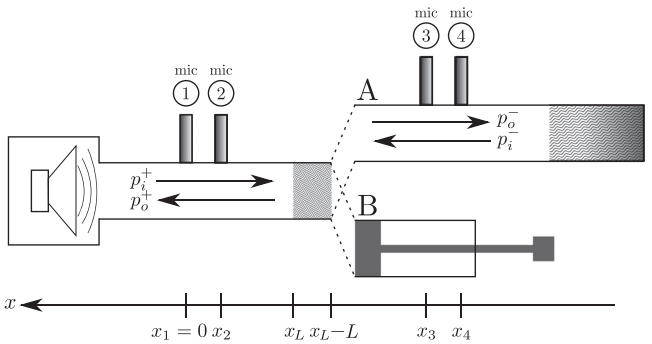

FIG. 1. Impedance tube configurations. A: transmission set-up. B: rigid backing.

Here the subscripts i and o denote the "incoming" and "outgoing" waves with respect to the sample. The plus and minus signs are used to denote the "left" and "right" domains on both sides of the sample in the tube, respectively, according to Fig. 1. The wavenumber k_t, and characteristic impedance Z_t, of the air inside the tube are complex valued and calculated with the Zwikker and Kosten formula[25,26] to account for the viscothermal losses on the tube boundary. Environmental conditions that were measured directly were atmospheric pressure P_0, temperature T_0, and relative humidity RH, from which the density of air ρ_0 can be calculated.

Now the scattering matrix can be written as

$$\begin{bmatrix} p_o^+ \\ p_o^- \end{bmatrix} = \begin{bmatrix} R & T' \\ T' & R \end{bmatrix} \begin{bmatrix} p_i^+ \\ p_i^- \end{bmatrix}, \tag{6}$$

where R and $T' = Te^{\mathrm{i}k_t L}$ are the reflection and transmission coefficients of a symmetric porous sample surrounded by air from both sides and L is the thickness of the sample. The pressures p in the scattering matrix Eq. (6) are standing wave pressures on the left and right surfaces of the sample. To find them, the standing wave amplitudes at x_1 are solved using Eq. (5), and the resulting pressures are multiplied with the appropriate propagation constant depending on the distance to the surface

$$p_i^+ = \frac{P_1 e^{-\mathrm{i}k_t x_1} - P_2 e^{-\mathrm{i}k_t x_2}}{e^{-2\mathrm{i}k_t x_1} - e^{-2\mathrm{i}k_t x_2}} e^{\mathrm{i}k_t |x_L|}, \tag{7a}$$

$$p_o^+ = \frac{P_1 e^{\mathrm{i}k_t x_1} - P_2 e^{\mathrm{i}k_t x_2}}{e^{2\mathrm{i}k_t x_1} - e^{2\mathrm{i}k_t x_2}} e^{-\mathrm{i}k_t |x_L|}, \tag{7b}$$

$$p_o^- = \frac{P_3 e^{-\mathrm{i}k_t x_3} - P_4 e^{-\mathrm{i}k_t x_4}}{e^{-2\mathrm{i}k_t x_3} - e^{-2\mathrm{i}k_t x_4}} e^{\mathrm{i}k_t (|x_L| + L)}, \tag{7c}$$

$$p_i^- = \frac{P_3 e^{\mathrm{i}k_t x_3} - P_4 e^{\mathrm{i}k_t x_4}}{e^{2\mathrm{i}k_t x_3} - e^{2\mathrm{i}k_t x_4}} e^{-\mathrm{i}k_t (|x_L| + L)}. \tag{7d}$$

Reflection and transmission coefficients for the symmetric porous sample can be solved from Eq. (6),

$$R = \frac{p_o^+ p_i^+ - p_o^- p_i^-}{(p_i^+)^2 - (p_i^-)^2}, \quad T' = \frac{p_o^- p_i^+ - p_o^+ p_i^-}{(p_i^+)^2 - (p_i^-)^2}. \tag{8}$$

Note that if the material was non-symmetric, the scattering matrix would include reflection coefficients R^+ and R^- of both sides of the sample. Now the characteristic impedance Z_m and wavenumber k_m of the material can be stated as[24,27]

$$Z_m = Z_t \sqrt{\frac{(1+R)^2 - T'^2}{(1-R)^2 - T'^2}}, \tag{9a}$$

$$e^{-\mathrm{i}k_m L} = \frac{T'(1-\tilde{z})}{R(1+\tilde{z}) - \tilde{z} + 1}, \tag{9b}$$

$$\Rightarrow k_m = -\frac{\ln\left(|e^{-\mathrm{i}k_m L}| + \mathrm{i}\mathrm{Arg}\left(e^{-\mathrm{i}k_m L}\right)\right)}{\mathrm{i}L} + \frac{2\pi n}{\mathrm{i}L}, \tag{9c}$$

where $\tilde{z} = Z_m/Z_t$ and $n \in \mathbb{N}$. The term $2\pi n$ exists to account for the phase wrap when inverting the k_m. Usually n is 0

because the measurements are performed in the low-frequency range.[13] Finally, we get[1]

$$\tilde{\rho}_{\mathrm{eq}} = Z_m k_m/\omega, \tag{10a}$$

$$\tilde{K}_{\mathrm{eq}} = Z_m \omega/k_m. \tag{10b}$$

B. Set-up B

In this configuration, the sample is placed on a rigid backing. We use set-up B in validating the measurements made in transmission mode, and to test the parameter inversion from reflection measurements only. Calculating the reflection coefficient R_{rigid} of the material with a rigid backing is done as in set-up A, except that now the pressures p_o^- and p_i^- are zero. Therefore,

$$R_{\mathrm{rigid}} = \frac{p_o^+}{p_i^+}. \tag{11}$$

IV. INVERSION

We describe the measurements in the impedance tube (set-up A) with the following observation model:

$$\boldsymbol{y} = h(\boldsymbol{\theta}, \boldsymbol{\xi}) + \boldsymbol{v}, \tag{12}$$

where $\boldsymbol{y} = [\tilde{\rho}_{\mathrm{eq}}^{\mathrm{meas}}, \tilde{K}_{\mathrm{eq}}^{\mathrm{meas}}]^\top$ denotes the measurements, $h(\boldsymbol{\theta}, \boldsymbol{\xi})$ is the forward model (JCAL) with $\boldsymbol{\theta} = [\phi, \alpha_\infty, \Lambda, \Lambda', k_0, k_0']$ the unknown parameters, and $\boldsymbol{\xi}$ the known variables (η, Pr, γ, ρ_0), and $\boldsymbol{v}$ is measurement noise. A brief discussion on inverting the parameters using the measurement configuration of set-up B is given in Appendix B.

We are looking for an estimate to $\boldsymbol{\theta}$ when $\boldsymbol{y}$ is known in two ways. First, we assume that the parameters and measurement noise are deterministic, i.e., they have constant values and no distribution. This leads to solving the least squares problem, which in the case of a nonlinear forward model is done iteratively. However, the solution returned by an iterative method should not be trusted without considering the possible sources of error. For example, the measured frequency range can be insufficient, leading to some parameters being highly correlated with each other. This can make them hard to separate reliably. Another danger is being trapped in a local minimum. In addition, we do not get estimates for the parameter uncertainty from this inversion process.

To answer the questions of parameter identifiability and correlation, one can view the problem in the Bayesian framework,[19] where each unknown is expressed as a random variable and the information on these variables is coded into probability distributions. The posterior probability density, i.e., the solution to this problem, allows the examination of spread and interdependence between the parameters in addition to point estimates. The statistical problem here is solved using numerical integration methods.

A. The deterministic problem

To solve the least squares problem, we first form the least squares (LS)-functional (or the "cost function"), as

$$\begin{aligned} f(\boldsymbol{\omega}; \boldsymbol{\theta}) &= \|\boldsymbol{y} - h(\boldsymbol{\theta}, \boldsymbol{\xi})\|^2 \\ &= W_1 \|\tilde{\rho}_{\mathrm{eq}}^{\mathrm{meas}}(\boldsymbol{\omega}) - \tilde{\rho}_{\mathrm{eq}}^{\mathrm{model}}(\boldsymbol{\omega}; \phi, \alpha_\infty, \Lambda, k_0)\|^2 \\ &\quad + W_2 \|\tilde{K}_{\mathrm{eq}}^{\mathrm{meas}}(\boldsymbol{\omega}) - \tilde{K}_{\mathrm{eq}}^{\mathrm{model}}(\boldsymbol{\omega}; \phi, \Lambda', k_0')\|^2, \end{aligned} \tag{13}$$

where $\boldsymbol{\omega}$ contains the angular frequencies, the minimization is carried over. The cost function is formed as a sum of the two functions $\tilde{\rho}_{\mathrm{eq}}$ and $\tilde{K}_{\mathrm{eq}}$ because they both contain information on ϕ and must therefore be minimized simultaneously. The weights $W_1 = 1/\rho_{\mathrm{RMS}}^2$ and $W_2 = 1/K_{\mathrm{RMS}}^2$ are added to make sure the density and bulk modulus have the same influence on the estimate of porosity. They are defined as $\rho_{\mathrm{RMS}} = \|\tilde{\rho}_{\mathrm{eq}}^{\mathrm{meas}}\|/\sqrt{N}$ and $K_{\mathrm{RMS}} = \|\tilde{K}_{\mathrm{eq}}^{\mathrm{meas}}\|/\sqrt{N}$, where N is the length of the frequency vector.

The solution of the minimization problem is

$$\hat{\boldsymbol{\theta}} = \arg\min_{\boldsymbol{\theta}} f(\boldsymbol{\omega}; \boldsymbol{\theta}), \tag{14}$$

and we solve it using the Nelder–Mead simplex algorithm,[28] which is an iterative method that uses only function evaluations and no derivatives. This method was chosen because it has been used in similar parameter inversion schemes.[29–32]

During the inversion, the parameters are bounded to physically reasonable values, $\phi \in [0, 1]$, $\alpha_\infty \in [1, 10]$, $\Lambda \& \Lambda' \in [10, 2000]$ μm, and $k_0 \,\&\, k_0' \in [0.1, 100] \cdot 10^{-9}\,\mathrm{m}^2$. In addition, two physical constraints[15] are provided: $\Lambda' \geq \Lambda$ and $k_0' \geq k_0$. The algorithm was run 30 times with initial guesses that were randomly varied within the parameter bounds to increase the chance of finding the global minimum. The result with the smallest LS-residual was chosen as the solution $\hat{\boldsymbol{\theta}}$.

B. The statistical problem

Statistical inversion is based on Bayes' formula, which states that the posterior probability density $\pi_{\mathrm{post}}(\boldsymbol{\theta}|\boldsymbol{y})$ is proportional to the prior density $\pi_{\mathrm{pr}}(\boldsymbol{\theta})$ multiplied by the likelihood $\pi(\boldsymbol{y}|\boldsymbol{\theta})$,

$$\pi_{\mathrm{post}}(\boldsymbol{\theta}|\boldsymbol{y}) \propto \pi(\boldsymbol{y}|\boldsymbol{\theta})\pi_{\mathrm{pr}}(\boldsymbol{\theta}). \tag{15}$$

Likelihood describes the relation between the model and the data and can also include information on the measurement noise and uncertainties. With the prior probability density, one can formally incorporate prior information into the inverse problem. This means knowledge on the parameters that has been obtained irrespective of the data $\boldsymbol{y}$. Informative priors shift the posterior towards the prior densities, but to better compare the method with the deterministic case, the prior densities we used in this work were uniform probability densities that do not carry much information. Their role was to set the same boundaries for each parameter as in the LS-problem (see Sec. IV A).

We model the measurement noise $\boldsymbol{v}$ in Eq. (12) as zero mean Gaussian with a covariance Γ_v, so $\pi_v \sim \mathcal{N}(0, \Gamma_v)$. It was also assumed that $\boldsymbol{v}$ and $\boldsymbol{\theta}$ are independent random variables. With these assumptions the likelihood can be written as[19]

$$\pi(\boldsymbol{y}|\boldsymbol{\theta}) = \pi_v(\boldsymbol{y} - h(\boldsymbol{\theta}, \boldsymbol{\xi})) \propto \exp\left\{-\frac{1}{2}(\boldsymbol{y} - h(\boldsymbol{\theta}, \boldsymbol{\xi}))^\top \Gamma_v^{-1}(\boldsymbol{y} - h(\boldsymbol{\theta}, \boldsymbol{\xi}))\right\}. \tag{16}$$

Because we consider the noise to be uncorrelated with the data, with a variance that is not dependent on the frequency, the covariance matrix is of the form

$$\Gamma_v = \begin{bmatrix} \Gamma_1 & 0 \\ 0 & \Gamma_2 \end{bmatrix}, \tag{17}$$

where $\Gamma_1 = \sigma_{\rho_v}^2 \rho_{\mathrm{RMS}}^2 I_N$ and $\Gamma_2 = \sigma_{\rho_K}^2 K_{\mathrm{RMS}}^2 I_N$. The sigmas σ_{ρ_v} and σ_{K_v} denote the standard deviations of the error, and I_N is the $N \times N$ identity matrix. Because all samples were measured in two orientations (the sample was turned around), we can obtain an estimate for the measurement error and noise standard deviation as the mean of the relative difference between the two measurements. Thus, the error standard deviation for the density for example is

$$\sigma_{\rho_v} = \mathrm{mean}\left(\left|\frac{\tilde{\rho}_{\mathrm{eq}}^{\mathrm{meas},1} - \tilde{\rho}_{\mathrm{eq}}^{\mathrm{meas},2}}{\tilde{\rho}_{\mathrm{eq}}^{\mathrm{meas},1}}\right|\right), \tag{18}$$

where the mean is taken over all the frequencies. Using this definition, the standard deviations range from less than 1% for the soft polyurethane foam to 10% for the fibrous samples. Another way to calculate σ_{ρ_v} would be to use the maximum value of the relative error, but due to effects of frame resonance (see Sec. V), the noise levels could be overestimated. The magnitude of the error standard deviation affects the width of the parameter spread estimates.

The final step, exploring the posterior density, is to calculate the desired statistics and point estimates. This is done using MCMC sampling, which we implemented using the Metropolis–Hastings algorithm[33,34] with an adaptive proposal distribution scheme.[20,21] This adaptive algorithm adjusts the size and spatial orientation of the proposal distribution considering all of the target distribution points accumulated so far, facilitating a faster convergence of the chain but also freeing the user from having to tune the proposal distribution by hand. We start the Markov chain at a location close to the LS-solution so that it should start mapping the real distribution quickly, and run it for 500 000 iterations with a burn-in of 50 000.

The point estimate for the parameters we use in this work is the maximum *a posteriori* (MAP) estimate, which corresponds to the point in the posterior that has the highest probability. If the presented LS-functional and posterior were constructed using the same ratios of weights for density and bulk modulus, and if both algorithms found the true minimum, the LS and MAP estimates would be equal. However, because in the construction of the likelihood we can give different noise standard deviations σ_{ρ_v} and σ_{K_v}, some differences are expected. As an indication of the uncertainty in the MAP-estimate, we use the standard deviation of the MCMC samples, which represents the spread of the posterior. It must be noted that if the parameter space is multi-modal, non-symmetric or if the MAP-estimate does not correspond to the mean of the chain, the standard deviation gives only a rough indication of the uncertainty. It is always beneficial to look at the one-dimensional and two-dimensional marginal densities directly.

V. RESULTS

The measured samples were five widely different porous materials, each with a diameter of 30 mm and thickness varying between 16 and 40 mm (see Fig. 2). The materials range from a soft polyurethane foam (SPF) with a flow resistivity of $\sigma \sim 2000$ Ns/m^4 to a wool with a flow resistivity of $\sigma \sim 60\,000$ Ns/m^4. The material frames were not stiffened by metal pins, so some elastic effects due to the viscous coupling between air and the frame are expected in the low-middle frequencies. The samples were measured in two ways, rotated around perpendicular to their axis, to validate their symmetry. The foam samples proved to give identical results when turned around implying that they are highly symmetric. The fibrous materials only provided close results, which is accounted for by a higher measurement error standard deviation [Eq. (18)] in the Bayesian inversion.

Pore parameter estimates given by the presented methods, along with an uncertainty estimate of one standard deviation of the MCMC samples (calculated from values after the burn-in) are shown in Table I. The estimated values are compared to a flow meter measurement,[4] to values given by an ultrasonic method,[35] and to parameters recovered with an analytical method.[11,12]

Figure 3 shows the real and imaginary parts of measured $\tilde{\rho}_{\mathrm{eq}}/\rho_0$, $\tilde{K}_{\mathrm{eq}}/P_0$, R, and T along with the reconstructed curves calculated using the MAP-estimate. The transition from isothermal to the adiabatic regime can be seen in the real part of $\tilde{K}_{\mathrm{eq}}/P_0$, going from approximately 1 to 1.4 when the porosity is close to unity. It seems that the transition happens at higher frequencies for materials which have a lower thermal permeability k_0'. This is supported by the fact that the thermal characteristic frequency ($\omega_{\nu'} = \phi\nu'/k_0'$) is inversely proportional to k_0'. The same is true for the viscous permeability k_0 and characteristic frequency $\omega_\nu = \phi\nu/(\alpha_\infty k_0)$. Thus when using the same absolute frequency range of measurements, a smaller part of the "full" behavior of the lower permeability materials is recorded, leading to grater uncertainties in the high frequency parameters. This partly explains why the estimate of Λ' is considerably more uncertain for the felt and wool samples.

Figure 3 also shows a measurement of the reflection coefficient R_{rigid} of the materials when they are put directly against a rigid backing (set-up B in the impedance tube). An

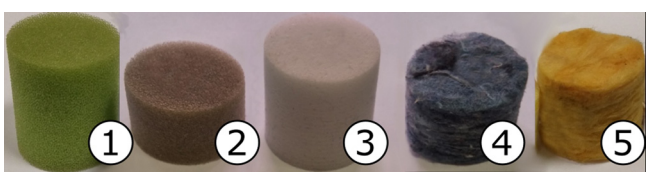

FIG. 2. (Color online) Samples used in this work. (1) SPF, (2) acoustic foam, (3) melamine foam, (4) felt, (5) glass wool.

TABLE I. Estimated values for the tested materials using the proposed LS and Bayesian (MAP-estimate and one standard deviation σ of the MCMC samples in brackets) approaches, the Olny and Panneton (OP) method,[11,12] and other measurements.[4,35] Also shown is the largest relative difference of each parameter over all samples, between the MAP-estimate and the OP and other methods.

Material	Method	ϕ	α_∞	Λ (μm)	Λ' (μm)	k_0 (10^{-9}m^2)	k_0' (10^{-9}m^2)
SPF	LS	1.00	1.04	273	550	8.94	14.30
	MAP (1σ)	1.00 (0.001)	1.04 (0.001)	273 (0.8)	549 (4)	8.94 (0.02)	14.37 (0.11)
	OP	-	1.06	296	347	8.84	13.19
	Other	0.98	1.05	289	-	10.22	-
Ac. foam	LS	0.97	1.16	133	231	3.10	6.55
	MAP (1σ)	0.97 (0.001)	1.16 (0.002)	133 (0.3)	231 (3)	3.11 (0.003)	6.56 (0.06)
	OP	-	1.17	129	235	3.26	7.03
	Other	0.99	1.12	101	-	3.57	-
Melamine	LS	1.00	1.00	107	198	1.26	2.82
	MAP (1σ)	1.00 (0.001)	1.00 (0.001)	106 (0.3)	197 (2)	1.26 (0.001)	2.82 (0.02)
	OP	-	1.00	119	150	1.26	2.81
	Other	0.97	1.00	138	-	1.45	-
Felt	LS	0.94	1.02	49	195	0.77	1.19
	MAP (1σ)	0.94 (0.01)	1.02 (0.02)	49 (2)	197 (47)	0.77 (0.003)	1.20 (0.07)
	OP	-	1.02	51	168	0.75	1.38
	Other	0.94	1.02	50	-	0.76	-
Wool	LS	0.96	1.00	37	100	0.39	0.58
	MAP (1σ)	0.96 (0.01)	1.00 (0.02)	37 (2)	99 (540)	0.39 (0.001)	0.58 (0.04)
	O-P	-	1.00	38	105	0.39	0.64
	Other	0.97	1.00	37	-	0.32	-
Max. relative	OP	-	2%	12%	37%	5%	15%
diff. to MAP	Other	3%	3%	30%	-	18%	-

analytically calculated reflection coefficient, using the MAP-estimate from Table I, is then plotted in the same figure. These lines show a good agreement and further validate the estimates.

As mentioned, the sharp deviations between the measured and modeled curves, visible especially in the glass wool and melamine around 2000 Hz, result from motion of the frame which is not accounted for in the JCAL model.

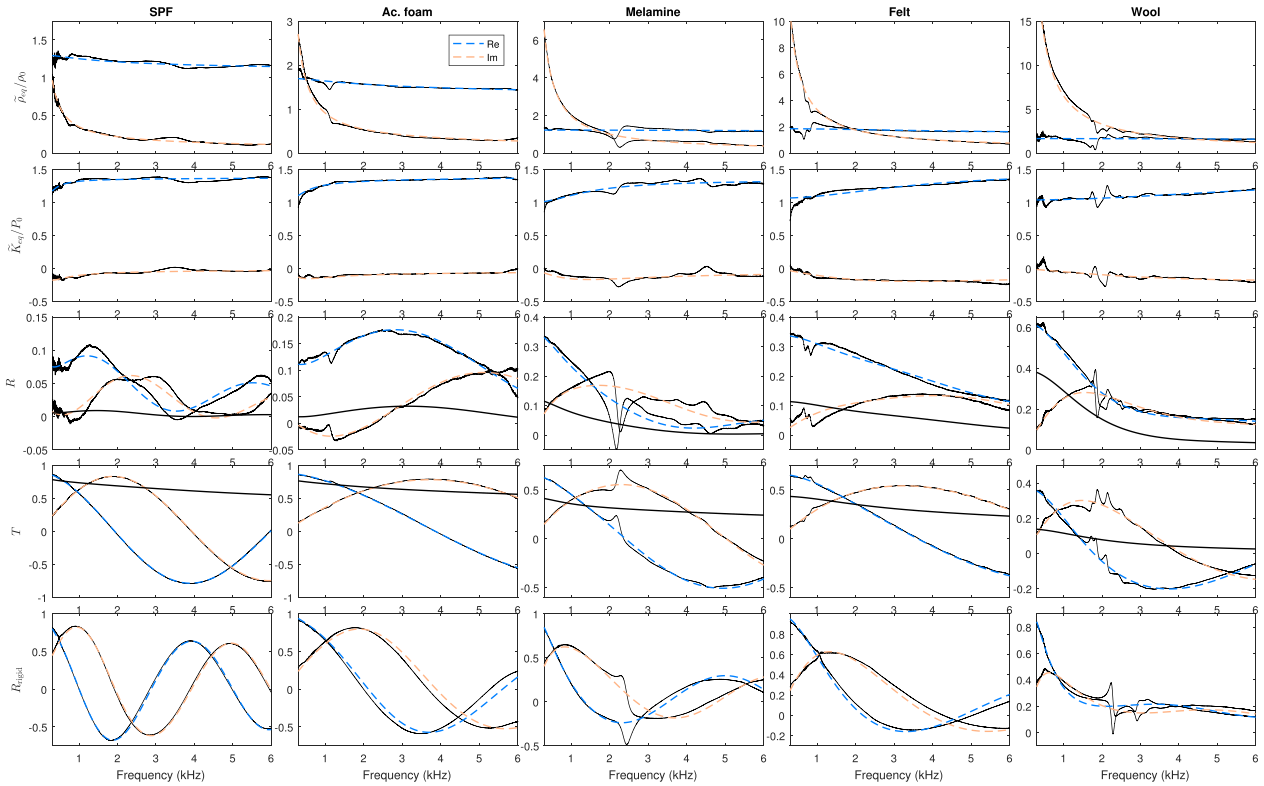

FIG. 3. (Color online) Real and imaginary parts of measured and recovered values of ρ/ρ_0, K/P_0, R and T. Thin black lines are the measurements, dotted lines are the reconstructed curves. The bottom row shows the reconstruction and measurement against a rigid backing. The thick black lines in R and T measurements show $|R|^2$ and $|T|^2$, respectively. Note that the y-axis changes from figure to figure for better visibility.

Most of the frame motion happens around the solid frame resonance that is defined by the material parameters and by the boundary conditions between the material and the tube. Above the resonance, there is partial decoupling between the frame and the fluid, and the acoustic wave propagating in the fluid phase cannot apply enough force to move the frame.[25] However, the overall effect of the frame resonance on the reconstruction is not too large since the peaks tend to be symmetric around the reconstructed curves and thus their effect on the cost function is partly cancelled out.

VI. DISCUSSION

An important reason for choosing to solve the problem in the Bayesian framework was to find out how ill-posed the inverse problem is, and whether the least squares solution is reliable. We discuss these points by examining the posterior.

Marginal densities of individual parameters (e.g., how are their probabilities distributed along the parameter space), and also the parameters' joint probability densities, can be calculated from the posterior density. Examining the joint probabilities gives information on the correlations between the parameters. This can be quantified for example with Pearson's correlation coefficient r, which measures linear correlation. It can be a useful test in estimating the quality of the parameter values, but also cannot replace visual examination of the data.

Figures 4–6 show two-dimensional marginal posterior densities of all JCAL parameters for SPF, acoustic foam, and glass wool. The posterior is represented by plotting some of the MCMC sample points, with 50 and 95% regions of distribution drawn around them. Also shown are the one-dimensional marginal densities, LS and MAP estimates, and the Pearson correlation coefficient r. The one- and two-dimensional marginal densities were calculated from the MCMC samples using kernel density estimation.[36]

We can immediately notice that the LS and MAP estimates are very similar (the maximum relative difference

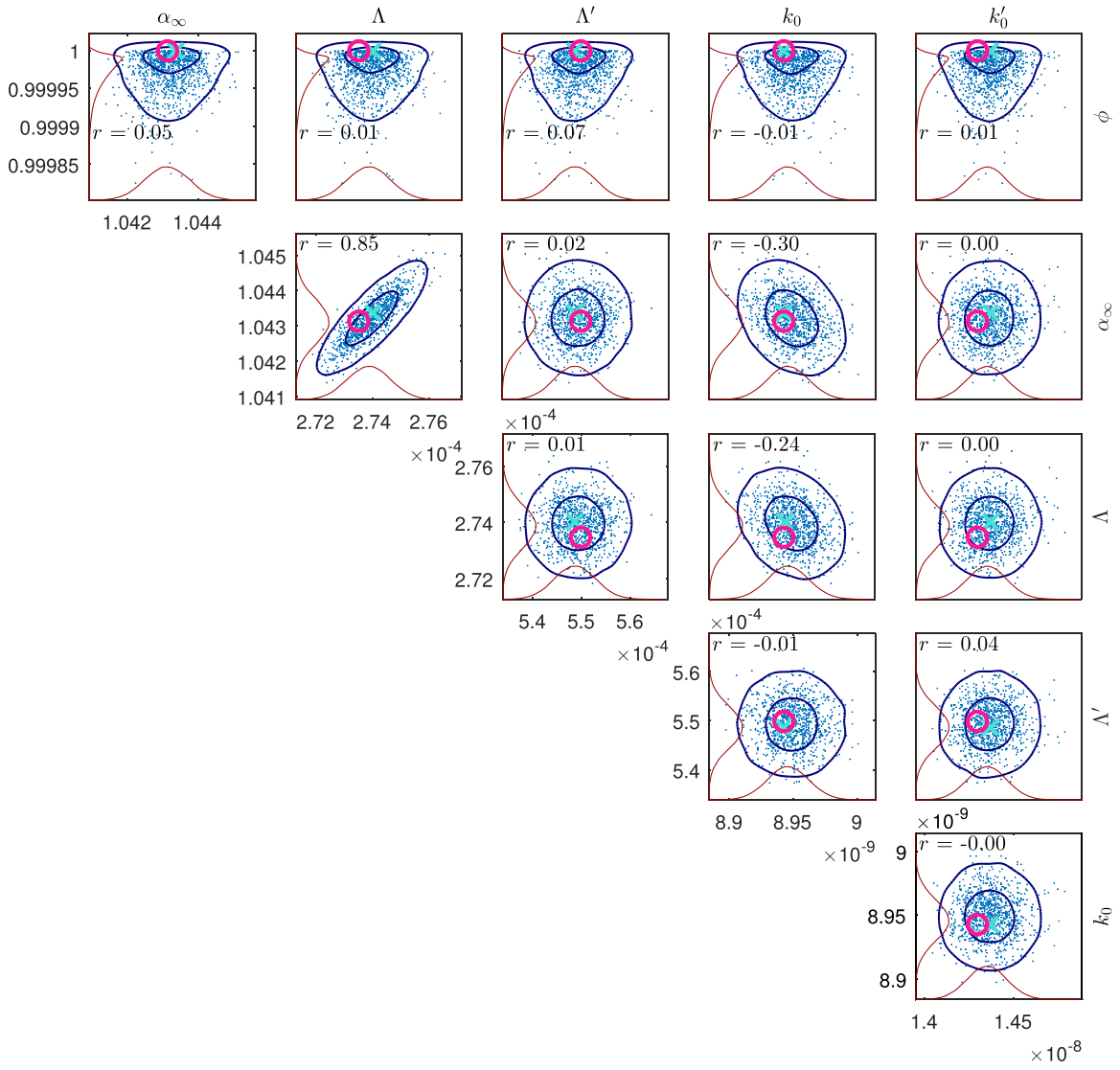

FIG. 4. (Color online) Two-dimensional marginal posterior densities of the soft polyurethane foam sample. The dots represent a sample of the MCMC points, the contours surrounding them show the 50 and 95% regions of distribution, and r is the Pearson correlation coefficient. The blue cross is the MAP-estimate, and the red circle is the LS-solution. The red curves on the bottom and left side of each plot are the one dimensional marginal posterior densities.

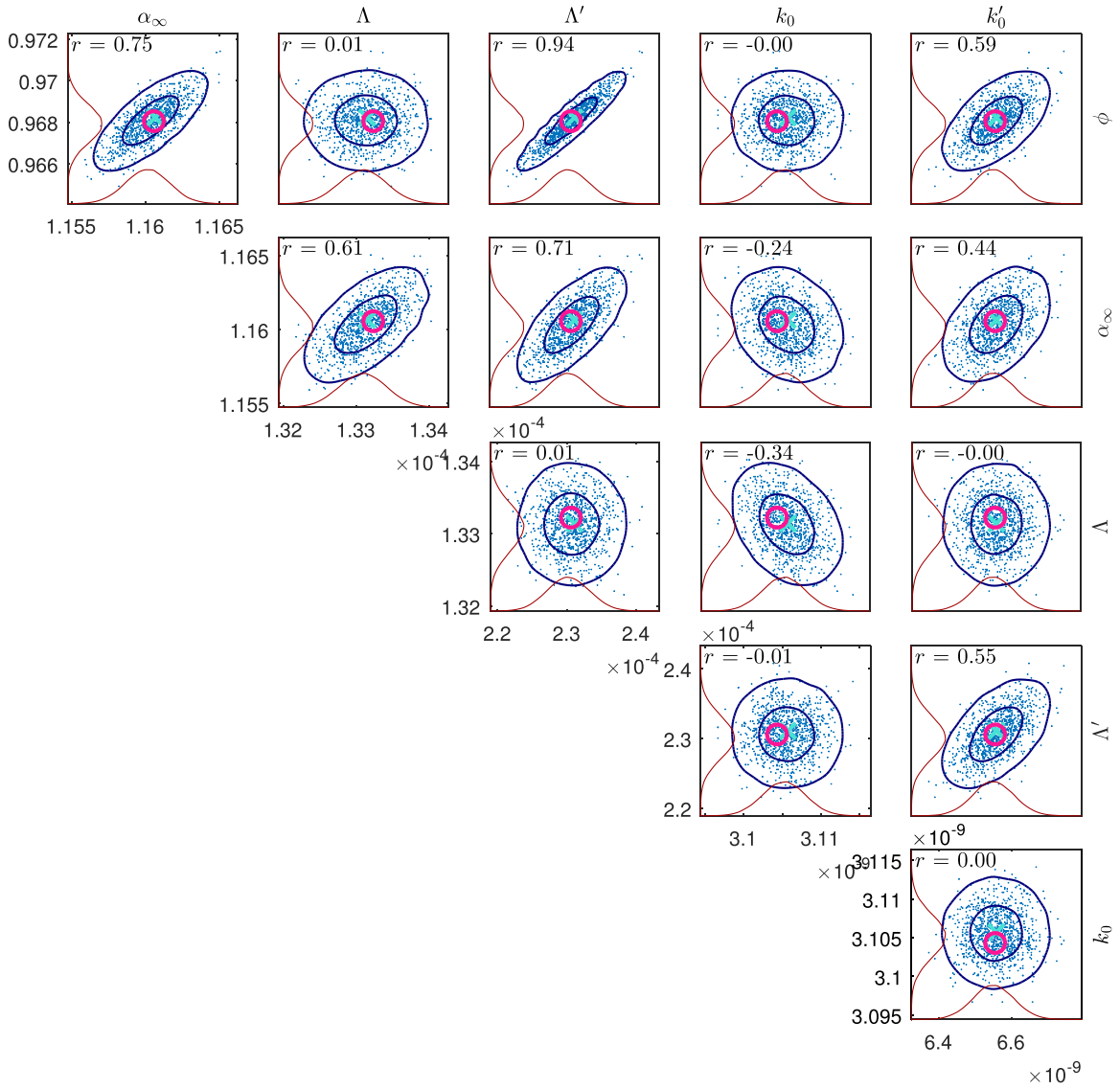

FIG. 5. (Color online) Two-dimensional marginal posterior densities of the acoustic foam sample.

is 1%), and the small differences can be attributed to the slightly different weighing of the density and bulk modulus parts of the cost function. The point estimates fall usually within the 50% region of the posterior mass. Most of the parameters seem to be uncorrelated, which can be seen by the nearly Gaussian shape of the joint density. However, some parameters such as tortuosity and viscous length, or porosity and thermal length, seem to depict correlation meaning they are not completely independent and their estimates can be more uncertain. The correlation between tortuosity and viscous length was also reported by Chazot *et al.*[8]

Due to the decoupling of viscous and thermal effects, most of the parameters are involved only in the expression for either density or bulk modulus, and the only common parameter between $\tilde{\rho}_{\mathrm{eq}} = \tilde{\rho}_{\mathrm{eq}}(\phi, \alpha_\infty, \Lambda, k_0)$ and $\tilde{K}_{\mathrm{eq}} = \tilde{K}_{\mathrm{eq}}(\phi, \Lambda', k_0')$ is the porosity. Therefore, no direct correlation between the viscous and thermal parameters is expected. There can be some correlation between a thermal and a viscous parameter if they are both correlated with porosity. This can be seen by looking at the joint marginal density of α_∞ and Λ' in Fig. 5, for example. In addition, there seems to be no (or very weak) correlation between the characteristic lengths and permeabilities. This shows that both parameters explain the behavior of the material independent of each other, which is logical since the permeabilities are defined as low-frequency and characteristic lengths as high-frequency parameters.

Posteriors of the foam-like materials show only one mode, but the posterior of glass wool seems to be more complicated. This is essentially the result of the thermal length Λ' being quite uncertain in the inversion, and it can have values up to the maximum specified upper limit of 2 mm. This can indicate that there is not enough information in the measurements (the frequency range is too small), or that the measurement uncertainty [Eq. (18)] is too large. Still, there exists a maximum point in the posterior, which also corresponds to the minimum in the LS-functional.

Seeing that some of the posteriors show multi-modality leads naturally to the question of whether the LS-solution

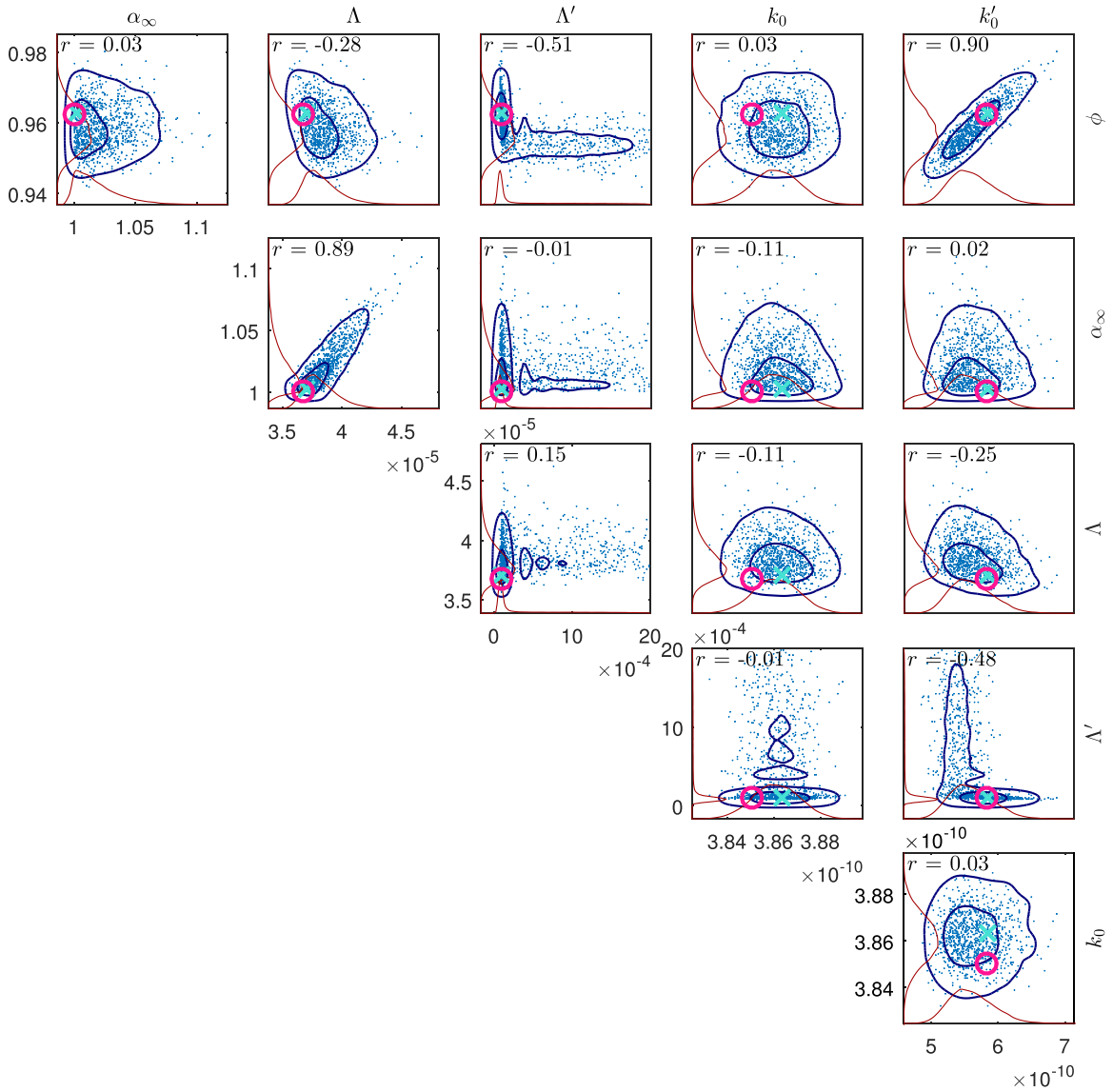

FIG. 6. (Color online) Two-dimensional marginal posterior densities of the glass wool sample.

finds the global minimum or gets trapped in some other mode. As mentioned in Sec. IV, this was examined by starting the iteration with several different values around the parameter space. For the foam materials the minimization method found the same (global) minimum every time. However, with the wool materials many different solutions were returned. Still, the global minimum (which we define as something close to the MAP-estimate, because it had the smallest LS-residual) was found after running the minimization enough times.

VII. CONCLUSION

A deterministic and a statistical method for recovering the physical parameters in the JCAL model were presented. Measurements were performed using equipment commonly found in acoustic laboratories, namely an impedance tube. The deterministic algorithm was based on minimizing the least squares residual between the measured and analytically calculated equivalent density and bulk modulus. Statistical inversion was carried out with the help of MCMC methods, using an additive noise model and an uninformative prior corresponding in principle to the LS definition. The information given by the statistical inversion was used to validate the use of the LS-method, and to quantify uncertainties in the parameter estimates.

We showed that the LS-method can be used to estimate the JCAL model parameters, but only when the automatic minimization process is run enough times so that the user can be confident to have found the global minimum. The obtained values were compared to a flow resistivity and ultrasonic measurements and to an analytical recovery process. Results indicated that the present methods can be used to recover all six parameters in the JCAL model with good accuracy. Moreover, they can be applied quickly to different materials since the process does not need user input, the parameters are recovered simultaneously, and none of the parameters (such as porosity or flow resistivity) need to be

known beforehand. All variables, including the characteristic lengths Λ and Λ', are recovered independently of each other, and we are also able to recover the thermal permeability k_0'.

The Bayesian methods can be extended to account for errors coming from other measurement uncertainties, improving the accuracy of the parameter uncertainty estimates. Such analysis, however, is out of the scope of this work. These uncertainties are associated for example to measurements of the sample thickness, and atmospheric conditions (temperature, humidity, pressure). The effect of the shearing resonance could also be taken into account using the Bayesian approximation error model[19] for example. Extending the Bayesian analysis further is a topic of future work.

ACKNOWLEDGMENTS

M.N., J.-P.G., A.D., O.D., J.-C.L.R., and N.P. gratefully acknowledge support from the RFI Le Mans Acoustique (Région Pays de la Loire) Decimap and PavNat projects. J.-P.G. and O.D. gratefully acknowledge support of the ANR Project METAUDIBLE (ANR-13-BS09-003) co-funded by ANR and FRAE. T. Lähivaara and T. Huttunen gratefully acknowledge support from the Academy of Finland (Project Nos. 257372 and 250215, Finnish Centre of Excellence in Inverse Problems Research) and from the strategic funding of the University of Eastern Finland. This article is based upon work from COST Action DENORMS CA-15125, supported by COST (European Cooperation in Science and Technology).

APPENDIX A: RESISTIVITY AND PERMEABILITY FORMULATIONS

The Johnson *et al.*[14] model can be written with the static flow resistivity σ by substituting the relation $k_0 = \eta/\sigma$ into Eq. (3)

$$\alpha(\omega) = \alpha_\infty + \frac{i\nu}{\eta\omega}\phi\sigma\sqrt{1 - \frac{i\eta^2\omega}{\nu}\left(\frac{2\alpha_\infty}{\phi\sigma\Lambda}\right)^2}. \tag{A1}$$

Similarly, by substituting $k_0' = \alpha_\infty\eta/\sigma'$ to the Lafarge *et al.*[16] model Eq. (4) and using the relation $\nu' = \eta/(\rho_0 \mathrm{Pr})$, we find the Champoux–Allard formulation [Eq. (19) of Ref. 15],

$$\tilde{\alpha}'(\omega) = 1 + \frac{i\sigma'\phi}{\rho_0\alpha_\infty \mathrm{Pr}\,\omega}\sqrt{1 - i\omega\eta\rho_0\mathrm{Pr}\left(\frac{2\alpha_\infty}{\sigma'\Lambda'\phi}\right)^2}. \tag{A2}$$

This substitution is analogous to making the assumption that the material consists of cylindrical pores and the Lafarge *et al.*[16] formulation shows that it is a valid assumption. However, it is preferable to use the k_0' form since Eq. (A2) includes tortuosity, a parameter dependent on direction that should not appear in the equation of bulk modulus, which is an isotropic quantity.

APPENDIX B: RIGID BACKING INVERSION

The measurement of the density and bulk modulus of the material requires measuring both transmission and reflection properties. A simpler approach would be to just use a two-microphone configuration (set-up B), where the sample is set on a rigid backing. This has also the advantage of supporting the sample meaning less frame resonance, but the drawback of having no information on the transmission properties and mixing the viscous and thermal parameters in the same expression.

The cost function is now formed as

$$f(\boldsymbol{\omega};\boldsymbol{\theta}) = \|R_{\mathrm{rigid}}^{\mathrm{meas}}(\boldsymbol{\omega}) - R_{\mathrm{rigid}}^{\mathrm{model}}(\boldsymbol{\omega};\boldsymbol{\theta})\|^2. \tag{B1}$$

Bayesian inversion is performed in the same way as detailed in Sec. IV, except that the likelihood now naturally includes only measurements of R_{rigid}, and $R_{\mathrm{rigid}}^{\mathrm{model}}(\boldsymbol{\omega};\theta)$ is calculated from the JCAL model with the recursive impedance formula.[1] Results of the inversion process for two samples are shown in Table II. Like with the transmission set-up inversion, the least squares solution was almost identical to the MAP-estimate and thus not shown here for easier comparison. Reaching the global LS minimum was however harder, since the Nelder–Mead algorithm returned several local minimum solutions even for the foam materials.

Even though some of the values recovered from rigid backing measurements are comparable to those recovered from $\tilde{\rho}_{\mathrm{eq}}$ & $\tilde{K}_{\mathrm{eq}}$, the estimates for the permeabilities and the thermal characteristic length seem to especially exhibit large discrepancies. In addition, for felt the inversion returns the same value for both Λ and Λ', which is only true when the width of the pore cross-section is constant. Figure 7 presents the marginal posterior densities of the felt sample. An interesting observation is that now the parameters are considerably more correlated than in the transmission tube case. These observations imply that it is preferable to use the transmission set-up and procedure related to $\tilde{\rho}_{\mathrm{eq}}$ & $\tilde{K}_{\mathrm{eq}}$ for the inversion.

TABLE II. MAP-estimates and one sigma uncertainties for SPF and felt using the proposed Bayesian approach from rigid backing measurements, and comparison to transmission measurement configuration.

Material	Method	ϕ	α_∞	Λ (μm)	Λ' (μm)	k_0 (10^{-9}m^2)	k_0' (10^{-9}m^2)
SPF	R_{rigid}	0.97 (0.002)	1.05 (0.001)	289 (3)	363 (9)	7.97 (0.15)	33.56 (15.4)
	$\tilde{\rho}_{\mathrm{eq}}$ & $\tilde{K}_{\mathrm{eq}}$	1.00 (0.001)	1.04 (0.001)	273 (0.8)	549 (4)	8.94 (0.02)	14.37 (0.11)
Felt	R_{rigid}	0.99 (0.006)	1.18 (0.03)	77 (6)	77 (5)	0.55 (0.006)	4.41 (29.0)
	$\tilde{\rho}_{\mathrm{eq}}$ & $\tilde{K}_{\mathrm{eq}}$	0.94 (0.01)	1.02 (0.02)	49 (2)	197 (47)	0.77 (0.003)	1.20 (0.04)

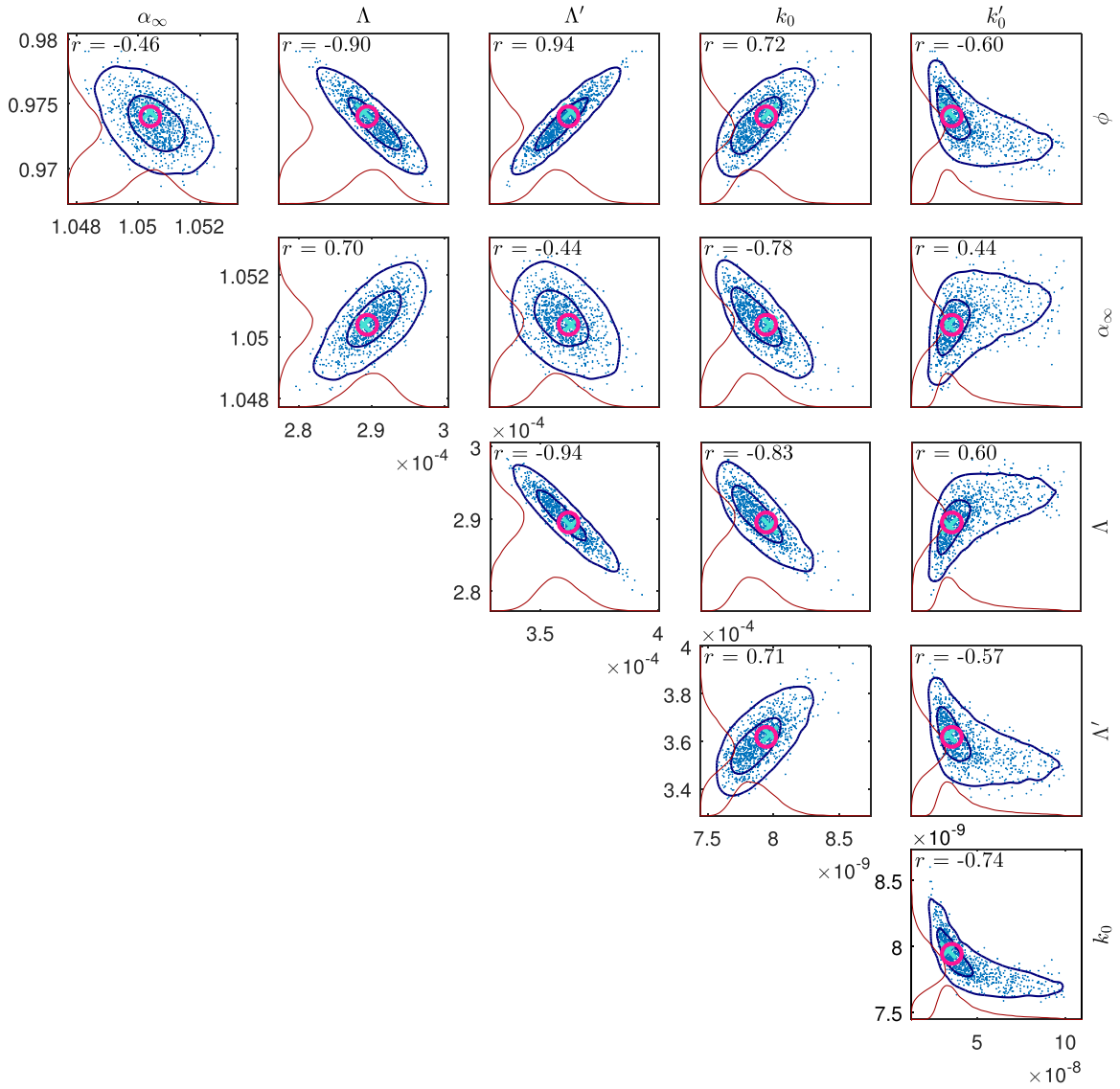

FIG. 7. (Color online) Two-dimensional marginal posterior densities of the soft polyurethane foam sample from rigid backing measurements.

[1]J.-F. Allard and N. Atalla, *Propagation of Sound in Porous Media: Modelling Sound Absorbing Materials*, 2nd ed. (John Wiley & Sons Ltd., Chichester, UK, 2009), pp. 1–358.

[2]K. V. Horoshenkov, "A review of acoustical methods for porous material characterization," Int. J. Acoust. Vib. **22**, 92–103 (2017).

[3]L. L. Beranek, "Acoustic impedance of porous materials," J. Acoust. Soc. Am. **13**, 248–260 (1942).

[4]R. L. Brown and R. H. Bolt, "The measurement of flow resistance of porous acoustic materials," J. Acoust. Soc. Am. **13**, 337–344 (1942).

[5]R. J. S. Brown, "Connection between formation factor for electrical resistivity and fluid-solid coupling factor in Biot equations for acoustic waves in fluid-filled media," Geophysics **45**, 1269–1275 (1980).

[6]Y. Champoux, M. R. Stinson, and G. A. Daigle, "Air-based system for the measurement of porosity," J. Acoust. Soc. Am. **89**, 910–916 (1991).

[7]Y. Atalla and R. Panneton, "Inverse acoustical characterization of open cell porous media using impedance tube measurements," Can. Acoust. **33**, 11–24 (2005).

[8]J.-D. Chazot, E. Zhang, and J. Antoni, "Acoustical and mechanical characterization of poroelastic materials using a Bayesian approach," J. Acoust. Soc. Am. **131**, 4584–4595 (2012).

[9]T. G. Zieliński, "Normalized inverse characterization of sound absorbing rigid porous media," J. Acoust. Soc. Am. **137**, 3232–3243 (2015).

[10]P. Leclaire, L. Kelders, W. Lauriks, M. Melon, N. Brown, and B. Castagnède, "Determination of the viscous and thermal characteristic lengths of plastic foams by ultrasonic measurements in helium and air," J. Appl. Phys. **80**, 2009–2012 (1996).

[11]R. Panneton and X. Olny, "Acoustical determination of the parameters governing viscous dissipation in porous media," J. Acoust. Soc. Am. **119**, 2027–2040 (2006).

[12]X. Olny and R. Panneton, "Acoustical determination of the parameters governing thermal dissipation in porous media," J. Acoust. Soc. Am. **123**, 814–824 (2008).

[13]J.-P. Groby, E. Ogam, L. De Ryck, N. Sebaa, and W. Lauriks, "Analytical method for the ultrasonic characterization of homogeneous rigid porous materials from transmitted and reflected coefficients," J. Acoust. Soc. Am. **127**, 764–772 (2010).

[14]D. L. Johnson, J. Koplik, and R. Dashen, "Theory of dynamic permeability and tortuosity in fluid-saturated porous media," J. Fluid Mech. **176**, 379–402 (1987).

[15]Y. Champoux and J. F. Allard, "Dynamic tortuosity and bulk modulus in air-saturated porous media," J. Appl. Phys. **70**, 1975–1979 (1991).

[16]D. Lafarge, P. Lemarinier, J. F. Allard, and V. Tarnow, "Dynamic compressibility of air in porous structures at audible frequencies," J. Acoust. Soc. Am. **102**, 1995–2006 (1997).

[17]K. V. Horoshenkov, A. Khan, F. X. Bécot, L. Jaouen, F. Sgard, A. Renault, N. Amirouche, F. Pompoli, N. Prodi, P. Bonfiglio, G. Pispola, F. Asdrubali, J. Hübelt, N. Atalla, C. K. Amédin, W. Lauriks, and L. Boeckx, "Reproducibility experiments on measuring acoustical properties of rigid-frame porous media (round-robin tests)," J. Acoust. Soc. Am. **122**, 345–353 (2007).

[18]F. Pompoli, , P. Bonfiglio, K. V. Horoshenkov, A. Khan, L. Jaouen, F. X. Bécot, F. Sgard, F. Asdrubali, F. D'Alessandro, J. Hübelt, N. Atalla, C. K.

Amédin, W. Lauriks, and L. Boeckx,"How reproducible is the acoustical characterization of porous media?," J. Acoust. Soc. Am. **141**, 945–955 (2017).
[19]J. P. Kaipio and E. Somersalo, *Statistical and Computational Inverse Problems* (Springer, Berlin, 2005), pp. 1–339.
[20]H. Haario, E. Saksman, and J. Tamminen, "Adaptive proposal distribution for random walk Metropolis algorithm," Comput. Stat. **14**, 375–396 (1999).
[21]H. Haario, E. Saksman, and J. Tamminen, "An adaptive Metropolis algorithm," Bernoulli **7**, 223–242 (2001).
[22]B. H. Song and J. S. Bolton, "A transfer-matrix approach for estimating the characteristic impedance and wave numbers of limp and rigid porous materials," J. Acoust. Soc. Am. **107**, 1131–1152 (2000).
[23]M. Åbom, "Measurement of the scattering-matrix of acoustical two-ports," Mech. Syst. Signal Process. **5**, 89–104 (1991).
[24]D. R. Smith, S. Schultz, P. Markoš, and C. M. Soukoulis, "Determination of effective permittivity and permeability of metamaterials from reflection and transmission coefficients," Phys. Rev. B **65**, 195104 (2002).
[25]C. Zwikker and C. W. Kosten, *Sound Absorbing Materials* (Elsevier, Amsterdam, 1949), pp. 1–174.
[26]M. R. Stinson, "The propagation of plane sound waves in narrow and wide circular tubes, and generalization to uniform tubes of arbitrary cross-sectional shape," J. Acoust. Soc. Am. **89**, 550–558 (1991).
[27]A. M. Nicholson and G. F. Ross, "Measurement of the intrinsic properties of materials by time-domain techniques," IEEE Trans. Instrum. Meas. **IM-19**, 377–382 (1970).
[28]J. C. Lagarias, J. A. Reeds, M. H. Wright, and P. E. Wright, "Convergence properties of the Nelder–Mead simplex method in low dimensions," SIAM J. Optim. **9**, 112–147 (1998).
[29]P. Bonfiglio and F. Pompoli, "Inversion problems for determining physical parameters of porous materials: Overview and comparison between different methods," Acta Acust. United Ac. **99**, 341–351 (2013).
[30]N. Sebaa, Z. E. A. Fellah, M. Fellah, E. Ogam, A. Wirgin, F. G. Mitri, C. Depollier, and W. Lauriks, "Ultrasonic characterization of human cancellous bone using the Biot theory: Inverse problem," J. Acoust. Soc. Am. **120**, 1816–1824 (2006).
[31]M. Sadouki, Z. E. A. Fellah, A. Berbiche, M. Fellah, F. G. Mitri, E. Ogam, and C. Depollier, "Measuring static viscous permeability of porous absorbing materials," J. Acoust. Soc. Am. **135**, 3163–3171 (2014).
[32]Z. E. A. Fellah, M. Sadouki, M. Fellah, F. G. Mitri, E. Ogam, and C. Depollier, "Simultaneous determination of porosity, tortuosity, viscous and thermal characteristic lengths of rigid porous materials," J. Appl. Phys. **114**, 204902 (2013).
[33]N. Metropolis, A. W. Rosenbluth, M. N. Rosenbluth, A. H. Teller, and E. Teller, "Equation of state calculations by fast computing machines," J. Chem. Phys. **21**, 1087–1092 (1953).
[34]W. Hastings, "Monte Carlo sampling using Markov chains and their applications," Biometrika **57**, 97–109 (1970).
[35]F. Fohr, D. Parmentier, B. R. J. Castagnede, and M. Henry, "An alternative and industrial method using low frequency ultrasound enabling to measure quickly tortuosity and viscous characteristic length," in *Proceedings of Acoustics 08*, Paris, France (June 30–July 4, 2008).
[36]Z. I. Botev, J. F. Grotowski, and D. P. Kroesse, "Kernel density estimation via diffusion," Ann. Stat. **38**, 2916–2957 (2010).